JACS
JOURNAL OF THE AMERICAN CHEMICAL SOCIETY
Communication
pubs.acs.org/JACS

General and Direct Method for Preparing Oligonucleotide-Functionalized Metal–Organic Framework Nanoparticles

Shunzhi Wang,[†,‡] C. Michael McGuirk,[†,‡] Michael B. Ross,[†,‡] Shuya Wang,[‡] Pengcheng Chen,[‡] Hang Xing,[†,‡] Yuan Liu,[†,‡] and Chad A. Mirkin*[,†,‡]

[†]Department of Chemistry and [‡]International Institute for Nanotechnology, Northwestern University, 2145 Sheridan Road, Evanston, Illinois 60208, United States

Supporting Information

ABSTRACT: Metal–organic frameworks (MOFs) are a class of modular, crystalline, and porous materials that hold promise for storage and transport of chemical cargoes. Though MOFs have been studied in bulk forms, ways of deliberately manipulating the external surface functionality of MOF nanoparticles are less developed. A generalizable approach to modify their surfaces would allow one to impart chemical functionality onto the particle surface that is independent of the bulk MOF structure. Moreover, the use of a chemically programmable ligand, such as DNA, would allow for the manipulation of interparticle interactions. Herein, we report a coordination chemistry-based strategy for the surface functionalization of the external metal nodes of MOF nanoparticles with terminal phosphate-modified oligonucleotides. The external surfaces of nine distinct archetypical MOF particles containing four different metal species (Zr, Cr, Fe, and Al) were successfully functionalized with oligonucleotides, illustrating the generality of this strategy. By taking advantage of the programmable and specific interactions of DNA, 11 distinct MOF particle–inorganic particle core–satellite clusters were synthesized. In these hybrid nanoclusters, the relative stoichiometry, size, shape, and composition of the building blocks can all be independently controlled. This work provides access to a new set of nucleic acid–nanoparticle conjugates, which may be useful as programmable material building blocks and as probes for measuring and manipulating intracellular processes.

It is known DNA is a versatile and powerful ligand for modifying nanomaterials, by virtue of its programmable and sequence-specific interactions.[1−3] For example, by densely functionalizing DNA onto spherical nanoparticles (NPs), one can orient the oligonucleotides (3′-5′ or 5′-3′) and generate spherical nucleic acid–nanoparticle conjugates (SNAs),[4] which exhibit unusual biological properties that have enabled a variety of applications in research and medicine. Indeed, many biodiagnostic systems and therapeutic lead compounds for gene regulation are now based upon SNAs.[5,6] In addition, they have become the central building blocks for crystal engineering approaches based upon the concept of DNA-programmable assembly.[7−9] Thus far, several approaches have been developed for modifying noble metal,[1,2,10] oxide,[11] quantum dot nanoparticles with DNA.[12] However, there are no general ways for directly modifying MOF nanoparticles with oligonucleotides in a preferential end-on manner. Indeed, all previous approaches have utilized either nonspecific interactions such as electrostatic adsorption and van der Waals interactions,[13,14] or required a coupling agent that is necessarily immobilized on the particle surface prior to functionalization with DNA,[15,16] rendering less control and generality.

Herein, we describe a general strategy for functionalizing MOF nanoparticles with oligonucleotides at high density. Using terminal phosphate-modified oligonucleotides, we can chemically address the dense coordinatively unsaturated metal sites (CUS) on a MOF nanoparticle surface.[17−21] Solid-state nuclear magnetic resonance (SSNMR) spectroscopy and powder X-ray diffraction (PXRD) confirm that the DNA-functionalization of MOFs occurs by metal–phosphate coordination and that the structural integrity and porosity of the MOF architecture are preserved postmodification (Scheme 1). As proof-of-concept of generality, this approach was extended to a series of nine different MOFs, featuring four metal nodes (Zr, Fe, Cr, Al) and four different organic linkers.

Scheme 1. (a) Schematic Representation of Solvothermal Synthesis of UiO-66 MOF Nanoparticles[a]; (b) DNA Modification of MOFs, Utilizing Terminal Phosphate-Modified DNA and Subsequent Sequence-Specific Assembly of MOF-NP Core–Satellite Hybrid architectures

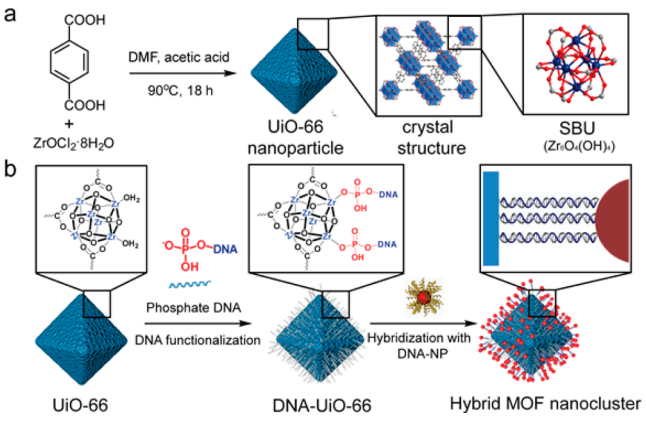

[a]Inset: $Zr_6O_4(OH)_4$ secondary building units (SBU).

Received: May 31, 2017
Published: July 18, 2017

DOI: 10.1021/jacs.7b05633
J. Am. Chem. Soc. 2017, 139, 9827−9830

For our initial study, UiO-66 was chosen due to its high stability and extensively characterized structure.[22] UiO-66 was synthesized under solvothermal conditions, using acetic acid to modulate crystallite size, resulting in 225 ± 35 nm (edge length) octahedral nanoparticles. The crystallinity and crystallite size of UiO-66 were determined by PXRD and scanning electron microscopy (SEM), respectively (Figure 1a,d). Next, phosphate-

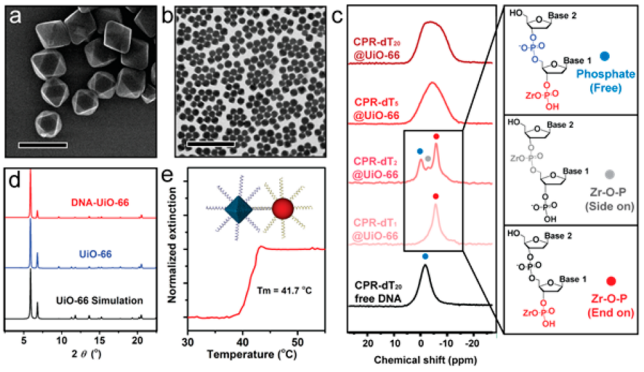

Figure 1. Characterization of DNA functionalized MOF nanoparticles: (a) SEM of UiO-66 and (b) TEM images of DNA functionalized UiO-66. (c) $^{31}P\{^{1}H\}$ SSNMR spectra of phosphate functionalized oligonucleotide. Inset: three phosphorus resonances corresponding to unbound phosphodiester (blue), side on Zr bound phosphodiester (gray) and Zr bound terminal phosphate (red). (d) PXRD of simulated UiO-66 (black), 225 nm UiO-66 before (red) and after (blue) DNA functionalization. (e) Melting transition of MOF and 50 nm gold nanoparticle aggregates assembled with complementary DNA. Scale bar = 500 nm in panel a and 2 μm in panel b.

modified nucleic acids were synthesized on a DNA synthesizer employing chemically modified phosphoramidites at either the 3′ or 5′ ends of the oligonucleotide. In a typical DNA-MOF particle functionalization experiment, excess oligonucleotide was added to a colloidal suspension of MOF nanoparticles, and subsequently incubated overnight (see SI). A salt-aging procedure was used to screen the negatively charged oligomers and achieve a high density of surface-immobilized oligonucleotides. Transmission electron microscopy (TEM) images and PXRD verified the shapes and crystallinity of the particles were preserved post-DNA modification (Figure 1b,d).

To confirm the immobilization of nucleic acids on the MOF nanoparticle surface, the interaction between terminal phosphate-functionalized DNA and Zr-based SBUs was probed using $^{31}P\{^{1}H\}$ magic angle spinning (MAS) solid-state NMR spectroscopy (Figure 1c). Oligo-T sequences, synthesized with a chemical phosphorylation reagent (CPR), with lengths of one base ("CPR-T_1"), two bases ("CPR-T_2"), and 20 bases ("CPR-T_{20}") were synthesized and chemically adsorbed onto MOF nanoparticles. As shown in Figure 1c, narrow phosphorus resonances centered at −0.3 ppm correspond to unbound phosphate in the free nucleic acid samples. In the CPR-T_1@UiO-66 case, Zr−phosphate bond formation was verified by a 4.8 ppm upfield shift in the phosphorus resonance from −0.3 to −5.1 ppm.[23] In the CPR-T_2@UiO-66 case, three resonances were observed and assigned to the P atom of the unbound phosphodiester (−0.2 ppm), the Zr−O−P (phosphodiester, −2.8 ppm), and Zr−O−P (terminal phosphate) resonance at −5.9 ppm (Figure 1c inset). The data suggest immobilization can occur two ways: end on and/or side on where both phosphates can bond with the Zr-rich surface. The significant peak intensity difference between two Zr−O−P modes (terminal phosphate vs phosphodiester) is due to the increased affinity of the terminal phosphate for the Zr centers as compared to that of the internal phosphodiester; this difference is primarily due to the increased steric hindrance felt by the internal phosphodiester and is in agreement with previous reports studying Zr−phosphate interactions, but not in the context of MOFs.[24] For CPR-dT_{20}@UiO-66, significant chemical shift broadening upon surface functionalization is observed. We attribute this change to the increased ratio of backbone to terminal phosphates, a distinct chemical environment for each backbone phosphate, and the greater degrees of freedom accessible for the longer oligonucleotide strand. Together, these data support the conclusion the terminal phosphate moiety of DNA coordinates to the previously solvent-bound Zr sites on the external surface of the MOF nanoparticles.

The extent of DNA coverage on the MOF surface was determined by inductively coupled plasma atomic emission spectroscopy (ICP-AES) and UV−visible spectroscopy (UV−vis). The surface area and Zr atoms per particle for UiO-66 were calculated based on a geometric approximation of the crystallite size, shape, and structure (see SI). To quantify the DNA surface coverage, Tamra dye-labeled DNA was used to modify UiO-66 particles. The absorption of Tamra at 556 nm was measured to determine that the average DNA loading on UiO-66 was 17 ± 6 pmol/cm^2, which correlates with the phosphorus and Zr concentrations measured by ICP-AES (see SI). The DNA surface coverage realized in this study is about two times higher than a report using a ligand strut modification approach.[15] The high DNA surface coverage was also confirmed by a thermal melting analysis of aggregates formed from DNA-functionalized UiO-66 nanoparticles and gold NPs (diameter = 50 nm) with complementary DNA, a property that is characteristic of particles with high DNA surface coverages.[1]

To evaluate the generality of this approach, nine distinct MOF architectures containing different metals and organic linkers were chosen, including UiO-66, UiO-67-bpy (2,2′-bipyridine-5′,5′-dicarboxylic acid), UiO-68-N_3/PCN-58, PCN-222/MOF-545, PCN-223, PCN-224, MIL-101 (Al), MIL-101 (Fe), and MIL-101 (Cr), representing four distinct metal nodes, four distinct organic linkers, and five different topologies (Figure 2). In addition to their high chemical stability, these MOFs show promise in nanomedicine.[25,26] MOF nanoparticle synthesis, characterization, and surface functionalization and quantification were carried out analogously to that described (Figures S1−6), following literature reports. In comparing these different MOFs, we tested how SBU density, SBU coordination number, and metal−oxygen bond dissociation energy affect surface functionalization.

We hypothesized DNA surface coverage would correlate with the density of SBUs present on the nanoparticle surface. To test this, three isoreticular Zr-based frameworks with the same underlying topology were synthesized, namely UiO-66, UiO-67-bpy, and UiO-68-N_3. Within this family, the density of surface metal nodes decreases as a function of increasing organic linker length, with the Zr oxide cluster SBU surface density (assuming (100) facet is exposed) estimated to be 0.27, 0.16, and 0.11 nm^{-2} for UiO-66, UiO-67-bpy, and UiO-68-N_3, respectively. As shown in Figure 2a, by plotting the DNA surface coverage as a function of Zr SBU density on each MOF surface, a linear relationship is observed, where the ratio of DNA to Zr SBU is essentially constant: structures with more surface Zr have more DNA. This is the first demonstration of a quantitative correlation between

DOI: 10.1021/jacs.7b05633
J. Am. Chem. Soc. 2017, 139, 9827−9830

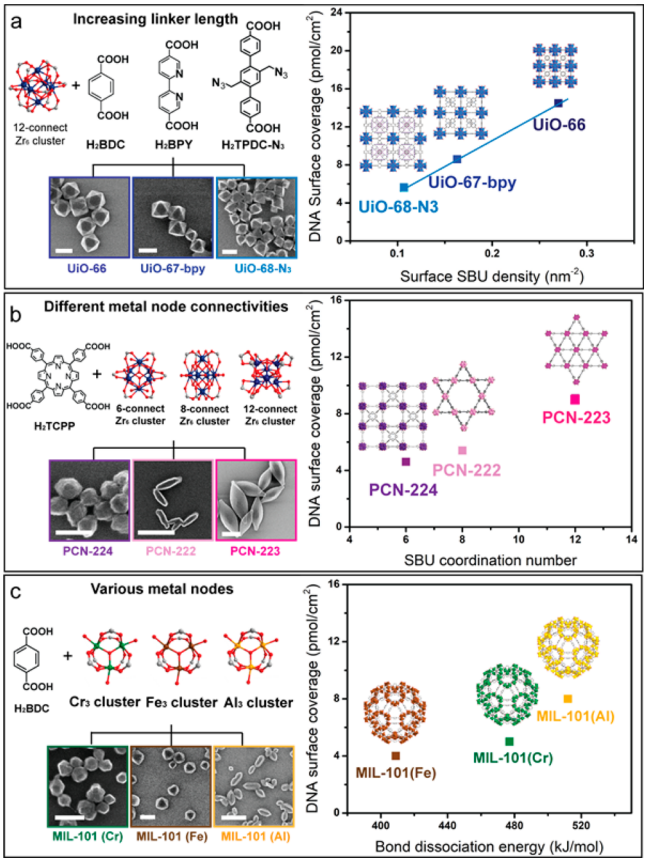

Figure 2. Library of nine MOFs synthesized and further functionalized with DNA. To systematically investigate factors affecting DNA surface coverage, (a) organic linker length, (b) metal node connectivity, and (c) type of metal cluster were independently and deliberately varied and DNA surface coverage was plotted against surface SBU density, SBU coordination number, and M−O bond dissociation energy. Scale bar = 200 nm.

DNA functionalization and surface SBU density on different MOFs, providing a way to select for MOF structures with the appropriate DNA surface loading for an intended use. Higher DNA loading density can significantly impact nanomaterial colloidal stability and certain biological applications where high DNA-loading is correlated with particle probe performance.

To test that MOFs with high SBU coordination numbers will result in higher DNA functionalization densities (due to more solvent-bound CUS on the nanoparticle surface), three Zr-based porphyrinic MOFs, PCN-222, PCN-223, and PCN-224, were synthesized from an identical tetracarboxyphenyl porphyrin linker (H_2TCPP). This resulted in structures that share different net topologies because of different SBU connectivity (Figure 2b). Specifically, three different octahedral Zr_6 SBUs with coordination numbers of 8-, 12-, and 6- define each of these frameworks, and yield comparable surface SBU densities of 0.28, 0.25, and 0.28 nm^{-2}, respectively. As shown in Figure 2b, a trend is seen where DNA surface coverage increases with SBU coordination number for three MOFs with comparable surface SBU density. This is because highly coordinated metal clusters expose higher degrees of surface defects due to coordination unsaturation,[27] which favors subsequent phosphate−DNA adsorption.

Next, we tested the formation of stronger metal−phosphate bonds will facilitate greater extents of DNA adsorption (SI Figure). Three isostructural MIL-101 frameworks were synthesized: MIL-101 (Cr), MIL-101 (Fe), and MIL-101 (Al). Because identical structures are found in all three MOFs, the importance of phosphate−metal bond strength (postadsorption) on determining DNA surface coverage can be evaluated. Metal−oxygen bond dissociation energies (BDE) of 409, 477, and 512 kJ/mol for the Fe−O, Cr−O, and Al−O bonds, respectively, have been reported.[28] An increase in DNA surface coverage as a function of BDE was observed (SI Figure).

Finally, with an understanding of the stability and density of the oligonucleotides at the DNA-MOF nanoparticle conjugate surface, we studied the hybridization and assembly properties of such structures with different DNA-NP sizes, shapes, and compositions. In particular, DNA-MOF nanoparticles and archetypical inorganic gold nanoparticle (AuNP) SNA conjugates were used to synthesize hybrid core−satellite nanoclusters. In a typical experiment, AuNPs of different sizes were functionalized with a DNA sequence complementary to those on the MOF nanoparticles to facilitate assembly, the compliments were mixed, salt-aged, and the resulting core−satellite hybrid architectures were isolated by low speed centrifugation. To confirm the morphology of the assembled nanoclusters, a developed silica encapsulation protocol for stabilizing DNA−nanoparticle assemblies was used, as shown in Figure 3a.[29] Importantly, no MOF-AuNP nanoclusters form upon mixing of noncomplementary DNA-functionalized particles.

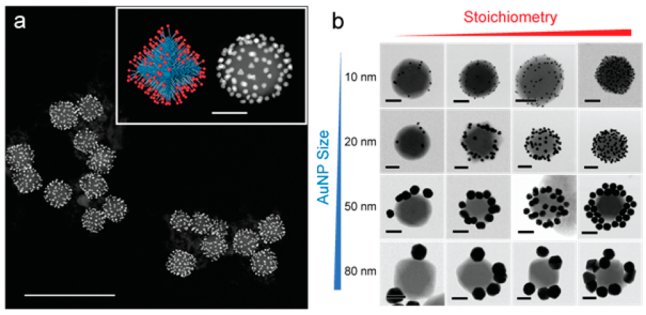

Figure 3. TEM and EDX characterization of DNA interconnected MOF NP-Au NP assemblies. (a) Representative HAADF image of nanoclusters formed from complementary 225 nm DNA-UiO-66 MOF NPs and 20 nm DNA-Au NPs. Inset: schematic illustration of a MOF NP-AuNP cluster, and a single nanocluster. (b) TEM images of nanocluster assemblies demonstrating how the programmable DNA ligands on MOF NPs and AuNPs provide control over the structural makeup of the assemblies (Au NP size and MOF-to-Au NP stoichiometry). All scale bars are 100 nm, except for in panel a, where it is 1 μm.

By modifying the stoichiometry of the DNA-mediated hybridization reaction (by varying MOF NP:AuNP ratio from 1:20 to 1:2000), the loading of metal NPs on the central MOF particle could be controlled (Figure 3b). The formation of MOF-NP nanocluster satellite structures is favored over polymeric structures at high AuNP:MOF ratios; once they form, they expose only identical noncomplementary DNA on the nanocluster periphery which inhibits the formation of extended networks via intercluster hybridization. To further explore the generality of this DNA-mediated approach, we systematically assembled satellite structures with MOF particle cores with a variety of DNA-functionalized NP building blocks, including gold nanostars, cubes, octahedra, and triangular prisms, silver spheres, and Fe_3O_4 spheres. TEM and energy-dispersive X-ray spectroscopy (EDX) mapping of the resulting structures show their clean formation (Figures S10 and 11). The cellular

DOI: 10.1021/jacs.7b05633
J. Am. Chem. Soc. 2017, 139, 9827−9830

cytotoxicity and uptake properties of MOF-NP hybrid nanoclusters were also assessed. The enrichment of MOF-AuNP nanocluster in cellular vesicles over time was demonstrated by confocal laser scanning microscopy (Figure S13), where strong accumulation of the nanocluster in cellular vesicle was observed as compared to an equivalent amount of single strand dye-labeled DNA, with no appreciable cytotoxicity (Figure S15). Together, the structures realized illustrate the versatility and potential utility of these new DNA-modified MOF NPs for programmable assembly and in applications where designer oligonucleotide interactions are relevant.

This work is important for the following reasons. First, it provides an approach to the synthesis of DNA-modified MOFs, independent of the choices of organic linkers and broadly applicable to a variety of metal clusters. Second, the structures realized are stable, have many of the original MOF characteristics, and can be programmably assembled with complementary DNA-modified NP building blocks. Third, design rules for modifying MOF NPs with DNA are emerging through this work. Most notably, we show DNA surface coverage directly correlates with MOF nanoparticle surface SBU density, coordination number, and metal−phosphate bond strength. Finally, the experiments described provide a route to a broad class of NP building blocks with tunable properties that can used to prepare designer materials with properties that may prove useful in biology,[30] catalysis,[31] and optics.[32]

■ ASSOCIATED CONTENT

Supporting Information

The Supporting Information is available free of charge on the ACS Publications website at DOI: 10.1021/jacs.7b05633.

Experimental materials, details, DNA sequences, and supplemental figures (PDF)

■ AUTHOR INFORMATION

Corresponding Author

*chadnano@northwestern.edu

ORCID

C. Michael McGuirk: 0000-0002-7420-1169
Michael B. Ross: 0000-0002-2511-0594
Pengcheng Chen: 0000-0002-0411-9549
Chad A. Mirkin: 0000-0002-6634-7627

Notes

The authors declare no competing financial interest.

■ ACKNOWLEDGMENTS

This material is based upon work supported by the following awards: Air Force Office of Scientific Research FA9550-14-1-0274, U.S. Army W911NF-15-1-0151, the IDP Sherman Fairchild Foundation through the Robert H. Lurie Comprehensive Cancer Center, and the National Science Foundation's MRSEC program (DMR-1121262) and made use of its Shared Facilities at the Materials Research Center of Northwestern University. Research reported in this publication was also supported by the National Cancer Institute of the National Institutes of Health under Award U54CA199091. The content is solely the responsibility of the authors and does not necessarily represent the official views of the National Institutes of Health.

■ REFERENCES

(1) Mirkin, C. A.; Letsinger, R. L.; Mucic, R. C.; Storhoff, J. J. *Nature* **1996**, *382*, 607.
(2) Alivisatos, A. P.; Johnsson, K. P.; Peng, X. G.; Wilson, T. E.; Loweth, C. J.; Bruchez, M. P.; Schultz, P. G. *Nature* **1996**, *382*, 609.
(3) Jones, M. R.; Seeman, N. C.; Mirkin, C. A. *Science* **2015**, *347*, 1260901.
(4) Cutler, J. I.; Auyeung, E.; Mirkin, C. A. *J. Am. Chem. Soc.* **2012**, *134*, 1376.
(5) Seferos, D. S.; Giljohann, D. A.; Hill, H. D.; Prigodich, A. E.; Mirkin, C. A. *J. Am. Chem. Soc.* **2007**, *129*, 15477.
(6) Rosi, N. L.; Giljohann, D. A.; Thaxton, C. S.; Lytton-Jean, A. K. R.; Han, M. S.; Mirkin, C. A. *Science* **2006**, *312*, 1027.
(7) Park, S. Y.; Lytton-Jean, A. K. R.; Lee, B.; Weigand, S.; Schatz, G. C.; Mirkin, C. A. *Nature* **2008**, *451*, 553.
(8) Nykypanchuk, D.; Maye, M. M.; van der Lelie, D.; Gang, O. *Nature* **2008**, *451*, 549.
(9) Macfarlane, R. J.; Lee, B.; Jones, M. R.; Harris, N.; Schatz, G. C.; Mirkin, C. A. *Science* **2011**, *334*, 204.
(10) Cai, H.; Xu, Y.; Zhu, N. N.; He, P. G.; Fang, Y. Z. *Analyst* **2002**, *127*, 803.
(11) Grancharov, S. G.; Zeng, H.; Sun, S. H.; Wang, S. X.; O'Brien, S.; Murray, C. B.; Kirtley, J. R.; Held, G. A. *J. Phys. Chem. B* **2005**, *109*, 13030.
(12) Zhang, C.; Macfarlane, R. J.; Young, K. L.; Choi, C. H. J.; Hao, L. L.; Auyeung, E.; Liu, G. L.; Zhou, X. Z.; Mirkin, C. A. *Nat. Mater.* **2013**, *12*, 741.
(13) Zhang, H. T.; Zhang, J. W.; Huang, G.; Du, Z. Y.; Jiang, H. L. *Chem. Commun.* **2014**, *50*, 12069.
(14) He, C. B.; Lu, K. D.; Liu, D. M.; Lin, W. B. *J. Am. Chem. Soc.* **2014**, *136*, 5181.
(15) Morris, W.; Briley, W. E.; Auyeung, E.; Cabezas, M. D.; Mirkin, C. A. *J. Am. Chem. Soc.* **2014**, *136*, 7261.
(16) Kahn, J. S.; Freage, L.; Enkin, N.; Garcia, M. A. A.; Willner, I. *Adv. Mater.* **2017**, *29*, 1602782.
(17) Hwang, Y. K.; Hong, D. Y.; Chang, J. S.; Jhung, S. H.; Seo, Y. K.; Kim, J.; Vimont, A.; Daturi, M.; Serre, C.; Ferey, G. *Angew. Chem., Int. Ed.* **2008**, *47*, 4144.
(18) Wang, S. Z.; Morris, W.; Liu, Y. Y.; McGuirk, C. M.; Zhou, Y.; Hupp, J. T.; Farha, O. K.; Mirkin, C. A. *Angew. Chem., Int. Ed.* **2015**, *54*, 14738.
(19) Roder, R.; Preiss, T.; Hirschle, P.; Steinborn, B.; Zimpel, A.; Hohn, M.; Radler, J. O.; Bein, T.; Wagner, E.; Wuttke, S.; Lachelt, U. *J. Am. Chem. Soc.* **2017**, *139*, 2359.
(20) McGuire, C. V.; Forgan, R. S. *Chem. Commun.* **2015**, *51*, 5199.
(21) Doonan, C.; Riccò, R.; Liang, K.; Bradshaw, D.; Falcaro, P. *Acc. Chem. Res.* **2017**, *50*, 1423.
(22) Cavka, J. H.; Jakobsen, S.; Olsbye, U.; Guillou, N.; Lamberti, C.; Bordiga, S.; Lillerud, K. P. *J. Am. Chem. Soc.* **2008**, *130*, 13850.
(23) Nakayama, H.; Eguchi, T.; Nakamura, N.; Yamaguchi, S.; Danjyo, M.; Tsuhako, M. *J. Mater. Chem.* **1997**, *7*, 1063.
(24) Nonglaton, G.; Benitez, I. O.; Guisle, I.; Pipelier, M.; Leger, J.; Dubreuil, D.; Tellier, C.; Talham, D. R.; Bujoli, B. *J. Am. Chem. Soc.* **2004**, *126*, 1497.
(25) Horcajada, P.; Chalati, T.; Serre, C.; Gillet, B.; Sebrie, C.; Baati, T.; Eubank, J. F.; Heurtaux, D.; Clayette, P.; Kreuz, C.; Chang, J. S.; Hwang, Y. K.; Marsaud, V.; Bories, P. N.; Cynober, L.; Gil, S.; Ferey, G.; Couvreur, P.; Gref, R. *Nat. Mater.* **2010**, *9*, 172.
(26) He, C. B.; Liu, D. M.; Lin, W. B. *Chem. Rev.* **2015**, *115*, 11079.
(27) Shearer, G. C.; Chavan, S.; Bordiga, S.; Svelle, S.; Olsbye, U.; Lillerud, K. P. *Chem. Mater.* **2016**, *28*, 3749.
(28) Cottrell, T. L. *The strengths of chemical bonds*; Butterworth Scientific Publications: London, 1954; p 310.
(29) Auyeung, E.; Macfarlane, R. J.; Choi, C. H. J.; Cutler, J. I.; Mirkin, C. A. *Adv. Mater.* **2012**, *24*, 5181.
(30) Langer, R.; Tirrell, D. A. *Nature* **2004**, *428*, 487.
(31) Brodin, J. D.; Auyeung, E.; Mirkin, C. A. *Proc. Natl. Acad. Sci. U. S. A.* **2015**, *112*, 4564.
(32) Bergman, D. J.; Stockman, M. I. *Phys. Rev. Lett.* **2003**, *90*, 90.

DOI: 10.1021/jacs.7b05633
J. Am. Chem. Soc. 2017, 139, 9827−9830